**Atmospheric
Chemistry
and Physics
Discussions**

Gas transport in firn: multiple-tracer characterisation and model intercomparison for NEEM, Northern Greenland

C. Buizert[1], P. Martinerie[2], V. V. Petrenko[3], J. P. Severinghaus[4], C. M. Trudinger[5], E. Witrant[6], J. L. Rosen[7], A. J. Orsi[4], M. Rubino[1,5], D. M. Etheridge[1,5], L. P. Steele[5], C. Hogan[8], J. C. Laube[8], W. T. Sturges[8], V. A. Levchenko[9], A. M. Smith[9], I. Levin[10], T. J. Conway[11], E. J. Dlugokencky[11], P. M. Lang[11], K. Kawamura[12], T. M. Jenk[1], J. W. C. White[3], T. Sowers[13], J. Schwander[14], and T. Blunier[1]

[1]Centre for Ice and Climate, Niels Bohr Institute, University of Copenhagen, Juliane Maries vej 30, 2100 Copenhagen Ø, Denmark
[2]Laboratoire de Glaciologie et Géophysique de l'Environnement, CNRS, Université Joseph Fourier-Grenoble, BP 96, 38 402 Saint Martin d'Hères, France
[3]Institute of Arctic and Alpine Research, University of Colorado, Boulder, CO 80309, USA
[4]Scripps Institution of Oceanography, Univ. of California, San Diego, La Jolla, CA 92093, USA

ACPD

11, 15975–16021, 2011

Gas transport in firn: multiple-tracer characterisation for NEEM

C. Buizert et al.

Title Page

Abstract	Introduction
Conclusions	References
Tables	Figures

|◀ | ▶|

◀ | ▶

Back | Close

Full Screen / Esc

Printer-friendly Version

Interactive Discussion

Abstract

Compacted snow (firn) preserves a continuous record of atmospheric composition up to a century back in time. Firn air transport modeling is essential for interpretation of firn gas records. Each site needs to be characterised individually through a tuning procedure, in which the effective diffusivity at each depth is adjusted to optimise the agreement between modeled and measured mixing ratios of a selected reference gas (usually CO_2). We present the characterisation of the NEEM site, Northern Greenland (77.45° N 51.06° W), where an ensemble of ten reference tracers is used to constrain the diffusivity reconstruction. By analysing uncertainties in both data and the reference gas atmospheric histories, we can objectively assign weights to each of the gases used for the model tuning, and define a root mean square criterion that is minimised in the tuning. Each tracer constrains the firn profile differently through its unique atmospheric history and free air diffusivity, making our multiple-tracer characterisation method a clear improvement over the commonly used single-tracer tuning. Six firn air transport models are tuned to the NEEM site; all models successfully reproduce the data within a 1σ Gaussian distribution. The modern day Δage, i.e. the difference between gas age and ice age, is calculated to be 182 ± 8 yr. We find evidence that diffusivity does not vanish completely in the firn lock-in zone, as is commonly assumed. We further present the first intercomparison study of firn air models, where we introduce diagnostic scenarios designed to probe specific aspects of the model physics. Our results show that there are major differences in the way the models handle advective transport. Furthermore diffusive fractionation of isotopes in the firn is poorly constrained by the models, which has consequences for attempts to reconstruct the isotopic composition of trace gases back in time using firn air and ice core records.

Title Page

Abstract | Introduction

Conclusions | References

Tables | Figures

◄ | ►

Back | Close

Full Screen / Esc

Printer-friendly Version

Interactive Discussion

1 Introduction

The compacted snow (firn) found in the accumulation zone of the major ice sheets acts as a unique archive of old air, preserving a continuous record of atmospheric composition from the present up to a century back in time (Battle et al., 1996). Sampling of this archive has allowed for reconstruction of the recent atmospheric history of many trace gas species (e.g. Butler et al., 1999; Sturrock et al., 2002; Aydin et al., 2004; Montzka et al., 2004; Assonov et al., 2007; Martinerie et al., 2009) and their isotopes (e.g. Francey et al., 1999; Ferretti et al., 2005; Bernard et al., 2006). Because of its temporal range it naturally bridges the age gap between direct atmospheric observations and the ice core record (Etheridge et al., 1998). Firn air analysis has some significant advantages over the ice core technique. First, firn air can be sampled directly using a pumping line (Schwander et al., 1993), making an ice extraction step unnecessary. Second, large sample sizes can be obtained making this method very suited for studying e.g. recent changes in the isotopic composition of trace gases (Sugawara et al., 2003; Röckmann et al., 2003; Ishijima et al., 2007). Third, because bubble occlusion introduces additional smoothing, firn air records can achieve higher temporal resolution than ice cores ().

Another important motivation for studying firn air is the interpretation of ice core records. All air found in glacial ice has first traversed the firn, and has thus been affected by its transport properties and the bubble close-off process. Some of the most commonly described artifacts of firn air transport are: gravitational fractionation (Craig et al., 1988; Schwander, 1989), thermal fractionation in the presence of temperature gradients (Severinghaus et al., 2001), diffusive smoothing of rapid atmospheric variations (Spahni et al., 2003), molecular size fractionation during bubble close-off (Huber et al., 2006; Severinghaus and Battle, 2006), diffusive isotopic fractionation (Trudinger et al., 1997) and Δage, the finite age difference between gas bubbles and their surrounding ice (Schwander et al., 1997). In certain cases the peculiarities of firn air transport actually give rise to new proxies, e.g. for temperature (Severinghaus and

Title Page

Abstract | Introduction

Conclusions | References

Tables | Figures

|◄ | ►|

◄ | ►

Back | Close

Full Screen / Esc

Printer-friendly Version

Interactive Discussion

Brook, 1999; Landais et al., 2004; Dreyfus et al., 2010) and local summer insolation (Kawamura et al., 2007).

Diffusion is the dominant mechanism by which variations in atmospheric composition are transferred into the firn. The effective diffusivity decreases with depth as the pore space decreases; unfortunately diffusivities measured on small firn samples do not adequately describe the behaviour of the whole firn (Fabre et al., 2000). Consequently the diffusivity profile with depth needs to be reconstructed for each firn air site independently through an inverse method (Rommelaere et al., 1997; Trudinger et al., 2002; Sugawara et al., 2003). The procedure consists of forcing a firn air transport model with the atmospheric history of a selected reference gas, often CO_2, and subsequently optimising the fit to measured mixing ratios in the firn by adjusting ("tuning") the effective diffusivity profile.

With few exceptions the firn air modeling studies found in literature tune their effective diffusivity profile to a single tracer. For the NEEM firn air site in Northern Greenland we have chosen to tune the effective diffusivity to an ensemble of ten tracers, namely CO_2, CH_4, SF_6, CFC-11, CFC-12, CFC-113, HFC-134a, CH_3CCl_3, $^{14}CO_2$ and $\delta^{15}N_2$. The studies by Trudinger et al. (1997, 2002); also use a wide variety of tracers, including halocarbons, greenhouse gases and radiocarbon ($\Delta^{14}C$), to characterise firn air transport. The main difference with these works is that we show how multiple tracers can be combined in a methodical tuning process. By systematically analysing all the uncertainties, both in the data and in the atmospheric histories of the references gases, we assign a unique weight to each data point in the tuning procedure. Using these uncertainty estimates we define an objective root mean square deviation (RMSD) criterion that is minimised in the tuning. We introduce tracers that have not previously been used in firn air studies, and provide atmospheric reconstructions for these species with realistic uncertainty estimates.

Our approach has several advantages. A central difficulty in reconstructing the diffusivity profile is that the problem is under-determined, with (infinitely) many solutions optimising the fit (Rommelaere et al., 1997). By adding more tracers, each with a

Title Page

Abstract | Introduction

Conclusions | References

Tables | Figures

◄ | ►►

◄ | ►

Back | Close

Full Screen / Esc

Printer-friendly Version

Interactive Discussion

(cc) BY

unique atmospheric history, the diffusivity profile is constrained more strongly. The final reconstructed profile is a trade-off between the demands of the different tracers. Second, many trace gases of interest, such as halocarbons, have a free air diffusivity that differs from CO_2 by up to a factor of 2. It is not a priori clear whether a profile tuned to CO_2 alone provides a good solution for these gases. The tracers in this study have a wide range of free air diffusivities, where the fastest tracer (CH_4) has a free air diffusivity that is three times that of the slowest one (CFC-113). Third, when using ten tracers the available dataset is much larger, with several data points at each sampling depth. This makes the final result more robust, i.e. less susceptible to effects of outliers and analytical biases. Finally, our method is less sensitive to errors in the reconstructed atmospheric history of individual reference gases. Our analysis shows that uncertainties in the atmospheric reconstruction are a large source of potential error.

Apart from presenting a new methodology for characterising firn air sites, this work will also serve as a reference for other studies using NEEM firn air. The modeling in a number of forthcoming publications in this issue will be based on the diffusivity reconstructions presented here.

We further present a model intercomparison between six state of the art one-dimensional firn air transport models. All the models are tuned to the same dataset, using the same physical firn parameters, such as porosity, free-air diffusion coefficients, etc. To diagnose model performance we introduce four synthetic scenarios that are designed to probe specific aspects of the model physics.

For many sections in this work more information is available in the Supplement. Because of the vast amount of material we have chosen to structure it the same as this work for easy referencing. Sections marked with an asterisk (*) in this work have a corresponding section in the Supplement where additional information can be found. The Supplement also includes all the firn air data and atmospheric reconstructions used in this study.

Title Page

Abstract	Introduction
Conclusions	References
Tables	Figures

◄◄ | ►►
◄ | ►

Back | Close

Full Screen / Esc

Printer-friendly Version

Interactive Discussion

2 Methods

2.1 NEEM 2008 firn air campaign[*]

The firn air used in this study was sampled during 14–30 July 2008 from two boreholes near the NEEM deep ice core drilling site, Northern Greenland (77.45° N 51.06° W).
5 The sampling site was 1.5 km outside of the main camp and chosen to avoid contamination by going upwind of the prevailing wind direction. The two boreholes, S2 and S3, were separated by 64 m. Firn air was sampled by drilling through the firn layers to the desired depth, and lowering the firn air sampling system into the borehole. The sampling system consists of a purge and sample line, running through an inflatable bladder
10 to seal off the firn air from the overlying atmosphere during sampling. S2 was sampled using the firn air system of the University of Bern (Schwander et al., 1993); S3 with the US firn air system (Battle et al., 1996). For this reason the boreholes are referred to as the "EU" and "US" holes, respectively. The CO_2 mixing ratio was monitored on the purge line with LICOR (US site) and MAIHAK (EU site) CO_2 analysers to assess
15 whether the firn air being pumped had been purged of modern air prior to sampling. A site map and a complete list of sampling depths can be found in the Supplement.

2.2 Physical characterisation of NEEM firn air site[*]

We use the assumption commonly made in firn air modeling that the firn density profile is in steady state, and that the site has been climatically stable over the study period.
20 For the firn density profile $\rho(z)$ we use an empirical fit to the NEEM main ice core density measurements averaged over 0.55 m segments (S. J. Johnsen, personal communication, 2009). For each of the three stages of the densification process (Arnaud et al., 2000) we use a combination of quadratic and exponential functions to fit the data, where care is taken that the derivative is continuous over the transitions between the
25 stages. The fit is generated on a $\Delta z = 0.2$ m grid, which is the spatial resolution used in this study. The density data and fit are shown in Fig. 1a. Following the temperature

Title Page

Abstract | Introduction

Conclusions | References

Tables | Figures

|◄ | ►|

◄ | ►

Back | Close

Full Screen / Esc

Printer-friendly Version

Interactive Discussion

Discussion Paper | Discussion Paper | Discussion Paper | Discussion Paper

relationship given by Schwander et al. (1997) a solid ice density $\rho_{ice} = 0.9206\,g\,cm^{-3}$ is used.

We use an accumulation rate of $A = 0.216\,m\,yr^{-1}$ ice equivalent as derived from the 2007 NEEM S1 shallow core (D. Dahl-Jensen, personal communication, 2010). Since the model runs cover the period 1800–2008 CE, we used the average rate over the same period as a best estimate. This long-term average is slightly lower than our best estimate for the current day accumulation of $0.227\,m\,yr^{-1}$ ice equivalent.

The total porosity $s = 1 - \rho/\rho_{ice}$ is divided into open and closed porosity (s_{op}, s_{cl}) using the parameterisation of Goujon et al. (2003):

$$s_{cl} = 0.37s\left(\frac{s}{s_{co}}\right)^{-7.6} \tag{1}$$

The deepest point at which firn air could be sampled successfully was $z = 77.75\,m$. The depth of total pore closure ($s_{op} = 0$) was determined experimentally in the field by drilling the EU hole to a depth of $z = 83\,m$, and subsequently raising the bladder in 0.5 m steps. The deepest point at which air could be pulled was $z = 79\,m$, though the flow was insufficient for sampling. To be consistent with this observation we use a mean close-off porosity $s_{co} = 9.708 \times 10^{-2}$ in Eq. (1), which leads to total pore closure ($s_{op} = 0$) at depth $z = 78.8\,m$, as shown in Fig. 1a.

We use an annual mean site temperature of $-28.9\,°C$ as obtained from borehole thermometry on the EU hole, and assume an isothermal firn for this modeling exercise. Atmospheric pressure is 745 hPa.

Traditionally the firn column is divided into three zones, based on the gravitational enrichment with depth (Sowers et al., 1992). For NEEM the $\delta^{15}N_2$ together with the zonal division is shown in Fig. 1b. Using the barometric line fitting method (Kawamura et al., 2006), we obtain a convective zone (CZ) thickness of 4.5 m. The zone below is called the diffusive zone (DZ), as diffusion dominates the transport at these depths. The lock-in depth is defined as the depth at which gravitational enrichment stops, which happens at $z = 63\,m$. Below we find the lock-in zone (LIZ), where advection with the

ice matrix dominates the transport. This is also the region where the majority of the bubble occlusion occurs, as can be seen from the s_{cl} curve.

2.3 Gas measurements[*]

A total of 345 samples were taken from the boreholes, with atmospheric samples taken
at three occasions during the sampling period. Different flask types were used (Silco-Can, stainless steel flasks and glass flasks); for the tracers used in this study no effect of flask type could be found in data comparison. We use firn air measurements from six different laboratories. The School of Environmental Sciences at the University of East Anglia (UEA) provided measurements of SF_6, CFC-11, CFC-12, CFC-113, HFC-134a,
CH_3CCl_3 on the EU borehole (Laube et al., 2010). NOAA Earth System Research Laboratory provided measurements of CO_2, CH_4 and SF_6 for both EU and US boreholes (Conway et al., 1994; Dlugokencky et al., 1994); the Institut für Umweltphysik at the University of Heidelberg (IUP) provided measurements of CO_2, SF_6 (both EU and US boreholes) and CH_4 (US borehole), (Levin et al., 2010, 2011); the Commonwealth
Scientific and Industrial Research Organisation, Marine and Atmospheric Research (CSIRO) provided CO_2 and CH_4 measurements for the EU borehole (Francey et al., 2003); the Australian Nuclear Science and Technology Organisation (ANSTO) provided $\Delta^{14}CO_2$ measurements for the EU borehole (Smith et al., 1999); the National Institute of Polar Research, Japan (NIPR) in collaboration with Scripps Institution of Oceanog-
raphy at the University of California, San Diego (SIO) provided measurements of $\delta^{15}N_2$ and $\delta^{86}Kr$ for both the EU and US boreholes (Severinghaus et al., 2003).

Where applicable, data from IUP were corrected for known calibration offsets to place all data on the NOAA scales used in the atmospheric reconstructions. After the calibration correction no systematic offsets were observed between the different laboratories.
As discussed below, there are significant offsets between the two boreholes, and data from the holes are not combined but treated separately. The $\Delta^{14}CO_2$ data and atmospheric reconstruction were both converted to a (mass conserving) ppm scale to allow $^{14}CO_2$ to be modeled like a regular tracer. Wherever multiple data points were available

for a certain depth they were averaged in the following order: first replicate measurements from one laboratory were averaged, then the resulting values from the different labs were averaged. In this way one composite dataset was created that contains 204 data points for the 10 tracers on the EU hole, and 77 data points for the 4 tracers on the

5 US hole. The $\delta^{15}N_2$ profile is the same for both holes, and a combination of EU and US depths are used in the final dataset. This gives a final dataset of 260 data points.

2.4 Reconstruction of atmospheric histories of selected tracers[*]

A best-estimate atmospheric history was reconstructed for each of the reference tracers used in the tuning. Additionally we reconstructed a $\delta^{13}CO_2$ history which was used

10 to convert the $\Delta^{14}CO_2$ reconstruction to a ppm scale (Stuiver and Polach, 1977). Four different types of data were used in the reconstructions:

   - Direct atmospheric measurements from sampling networks or archived air. Northern Hemisphere high latitude stations (i.e. Alert, Summit and Barrow) are used whenever available. When using data from other stations a correction should be made to

15 account for the latitudinal gradient. This is done whenever the gradient could be reliably determined. We used station data from the NOAA-ESRL network for CO_2, CH_4, SF_6 and HFC-134a (Conway et al., 1994; Dlugokencky et al., 1994; Geller et al., 1997; Montzka et al., 1996); from ALE/GAGE/AGAGE for CFC-11, CFC-12, CFC-113 and CH_3CCl_3 (Prinn et al., 2000, 2005; Cunnold et al., 1997; Fraser et al., 1996); from

20 CSIRO for $\delta^{13}CO_2$ (Francey et al., 2003). All ALE/GAGE/AGAGE data were converted to NOAA calibrations scales; all $\delta^{13}CO_2$ data are kept on the CSIRO calibration scale. Furthermore we used the SIO Mauna Loa record for CO_2 between 1958–1985 CE (Keeling et al., 2009), and the Cape Grim air archive for $\delta^{13}CO_2$ between 1978–1991 (Francey et al., 1999). The $^{14}CO_2$ history between 1963–1993 is based on Fruholmen,

25 Norway, for its proximity to Greenland (Nydal and Lövseth, 1996); data from other stations were used to complete time coverage (Manning and Melhuish, 1994; Levin and Kromer, 2004; Levin et al., 2008).

– High resolution firn air/ice core measurements from the high accumulation Law Dome sites, Antarctica. The reconstructions of CO_2 before 1958, and CH_4 before 1983 are based on Etheridge et al. (1996, 1998) and MacFarling Meure et al. (2006); $\delta^{13}CO_2$ before 1976 is based on Francey et al. (1999).

5 – Dendrochronologically-dated tree-ring measurements of radiocarbon. The reconstruction of atmospheric $^{14}CO_2$ before 1955 is based on Reimer et al. (2004).

– Emission-based estimates using a 2-D atmospheric transport model that includes latitudinal source and sink distribution (Martinerie et al. (2009) and references therein). This has been used to complete time coverage for SF_6 and halocarbons
10 before the onset of direct atmospheric measurements.

All the atmospheric reconstructions start in the year 1800 and have monthly resolution. We use 2008.54 (mid July) as the decimal sampling date in the models. Where applicable the reconstructions were converted to the most recent NOAA scale to be consistent with the data. Both data and atmospheric reconstructions are documented
15 and provided in the Supplement.

2.5 Gravitational correction[*]

The gravitational fractionation of gases in the firn column with depth, $\delta_{grav}(z)$, is well established both theoretically and experimentally (Craig et al., 1988; Schwander, 1989; Sowers et al., 1992). All data used in this study, with the exception of $^{15}N_2$, have been
20 corrected for the effect of gravity prior to the modeling. Consequently the models are run with either the molecular weight of all gases set equal to that of air ($M = M_{air}$) or gravity set to zero ($g = 0$). Since the correction is based on actual measurements of $\delta^{86}Kr$ ($^{86}Kr/^{82}Kr$), this procedure ensures the effect of gravity is included correctly. When, on the other hand, the effect of gravity is handled by the model, errors can be
25 introduced when the modeled $\delta_{grav}(z)$ deviates from the true observed values.

2.6 Differences between the EU and US boreholes

Though the boreholes are separated by a mere 64 m, within the lock-in zone we find differences in the mixing ratio profiles for CO_2, CH_4 (Fig. 2) and SF_6 (not shown) that exceed the estimated uncertainty of the combined sampling-measurement procedure
5 (indicated with errorbar, see Sect. 2.7 for details). Note that we cannot make the same comparison for the other gas species since only data from the EU hole are available. We attribute these differences to lateral inhomogeneity in the firn stratigraphy, possibly originating from surface wind features that have been preserved in the densification process. Because of these differences we have chosen to model both holes separately.
10 For SF_6 we furthermore observe a ~ 0.25 ppt offset in the 5–50 m depth range, contrary to the CO_2 and CH_4 profiles that agree well between the holes at these depths. This excludes differences in age distribution of the air as the origin. Alternative explanations we considered, such as incomplete flask flushing, sample contamination, procedural blanks and bladder outgassing, could all be excluded. Since we found no
15 objective reason to reject data from either hole, we account for the discrepancy by assigning an additional errorbar to the SF_6 data from both holes in this depth range (see below).

2.7 Full uncertainty estimation[*]

Having accurate uncertainty estimates is essential for our multiple-tracer methodology.
20 A unique uncertainty estimate has been assigned to each of the 260 individual data points used in this study based on the following seven potential sources of uncertainty: (1) analytical precision as specified by the laboratories. (2) Uncertainty in atmospheric reconstructions. (3) Contamination with modern air in the deepest firn samples; the estimates are based on HFC-134a, SF_6 and CFCs, which should be absent in the deep-
25 est samples. (4) Sampling effects estimated from inter-laboratory and inter-borehole offsets. (5) Possibility of in-situ CO_2 artifacts (e.g. Tschumi and Stauffer, 2000) and CO_2 enrichment due to close-off fractionation (Huber et al., 2006; Severinghaus and

Printer-friendly Version

Interactive Discussion

Battle, 2006). (6) Undersampling of seasonal cycle in the monthly atmospheric reconstruction (CO_2 only). (7) Large unexplained EU-US borehole difference in the diffusive zone (SF_6 only).

The errors are assumed to be independent of each other. The uncertainties in the atmospheric reconstructions are converted from a time- to a depth scale by running them through the CIC firn air model. Details are given in the Supplement. For most tracers the atmospheric reconstruction is the largest contributor to the total uncertainty.

3 Modeling firn air transport at NEEM

3.1 Tuning of the diffusivity profile[*]

How the diffusive transport changes with depth needs to be reconstructed through an inverse method for each firn air site independently. The procedure consists of forcing the transport models with the atmospheric history of one or several selected reference tracer(s), and subsequently optimising the fit to the measured mixing ratios in the firn by adjusting the effective diffusivity values at each depth (Rommelaere et al., 1997; Trudinger et al., 2002; Sugawara et al., 2003).

Here we will use diffusion as a generic term for mass transfer processes that are driven by a concentration gradient, and well described by Fick's law. The diffusivity profile we reconstruct is composed of two parts:

Molecular diffusion is a microscopic process originating in the thermal motion of the molecules constituting the firn air. The effective molecular diffusion coefficient of gases in the open porosity decreases with depth as the diffusive path becomes increasingly tortuous due to the densification process (Schwander et al., 1988). The diffusion coefficient of gas X at depth z is given by

$$D_X(z) = \frac{D_X^0}{\tau(z)} = \gamma_X \frac{D_{CO_2}^0}{\tau(z)} \tag{2}$$

15987

where D_X^0 is the diffusion coefficient in free air, $\tau(z)$ is the tortuosity at depth z, and $\gamma_X = D_X/D_{CO_2}$ is the ratio of diffusion coefficients (Trudinger et al., 1997). It is clear from Eq. (2) that the molecular diffusivity profiles for the different gas species scale linearly with each other. The γ_X used in this study are based on measurements by Matsunaga et al. (1993, 1998, 2002a,b), or a theoretical formula (Chen and Othmer, 1962) for gas species where no experimental data are available. Values can be found in the Supplement.

Eddy diffusion refers to mass transfer caused by macroscopic flow patterns in the open porosity which the models cannot resolve directly, and are instead parameterised through the inclusion of a diffusion coefficient $D_{eddy}(z)$. Unlike molecular diffusion, D_{eddy} is equal for all gases as the process is macroscopic in origin. The first contribution to D_{eddy} is convective mixing in the top few meters due to seasonal temperature gradients and wind pumping (Colbeck, 1989; Severinghaus et al., 2001; Kawamura et al., 2006). Furthermore, some of the models include dispersion in deeper firn layers arising from a non-uniform velocity distribution and viscous flow in the pores. The average velocity w_{air} at which gases are advected downwards relative to the surface can be derived from considerations of mass conservation and the porosities s_{op} and s_{cl}. w_{air} is lower than the downward ice velocity $w_{ice} = A\rho_{ice}/\rho$ due to the relative upward flow caused by compression of open pores (Rommelaere et al., 1997; Sugawara et al., 2003). A cul-de-sac, or relatively isolated air pocket within the open porosity provides one possibility for dispersive mixing. Part of the air in the pocket will be advected downwards at a velocity $w = w_{ice} > w_{air}$. Part will be squeezed out into the overlying pore space due to firn compaction, and be transported at a velocity $w < w_{air}$. This spread in velocities results in dispersive mixing. Additionally, low frequency pressure fluctuations at the surface can move around air at depth (Schwander, 1989). These macroscopic flow patterns cause dispersive mixing due to the finite viscosity of the air.

The extensive uncertainty analysis we introduced in Sect. 2.7 assesses how reliable each data point is, and consequently how much weight should be assigned to it in the tuning procedure. This allows us to combine multiple tracers in the tuning, and the

final reconstructed diffusivity profile is a trade-off between the constraints placed by the different tracers. All models in this study tuned their effective diffusivity profiles as to minimise the root mean square deviation

$$\text{RMSD} = \left(\frac{1}{N} \sum_{i=1}^{N} \frac{(m_i - d_i)^2}{\sigma_i^2} \right)^{\frac{1}{2}} \tag{3}$$

5 where the d_i are the measured data points for a given borehole (all tracers), m_i are the linearly interpolated modeled values at the same depth, and σ_i give the total uncertainties. The index i runs over all data points, where $N = 204$ for the EU hole, and $N = 77$ for the US hole.

3.2 Model description[*]

10 Six 1-D firn air transport models are tuned to the NEEM 2008 firn air data in the way outlined above. The models (in alphabetical order) were developed at the Centre for Ice and Climate (CIC), Commonwealth Scientific and Industrial Research Organisation (CSIRO, Trudinger et al., 1997), Institute of Arctic and Alpine Research (INSTAAR), Laboratoire de Glaciologie et Géophysique de l'Environnement and Grenoble Image
15 Parole Signal Automatique (LGGE-GIPSA, abbreviated as LGGE in figure legends, Witrant et al., 2011), Oregon State University (OSU) and the Scripps Institution of Oceanography (SIO, Severinghaus and Battle, 2006).

Table 1 summarises a selection of relevant model characteristics. The second column indicates the kind of coordinate system used by each model. The CSIRO model
20 is unique in using a coordinate system that moves downwards with descending ice layers (Lagrangian coordinates), giving a downward ice velocity $w_{\text{ice}} = 0$ relative to the reference frame. The other models use a static (Eulerian) coordinate system where the surface stays at $z = 0$ and the ice layers move down at a finite velocity $w_{\text{ice}} = A\rho/\rho_{\text{ice}}$. The choice of coordinate system has consequences for the way advection of air with
25 the ice matrix is handled (third column). In the CSIRO model the moving coordinate

system automatically leads to advective transport without the need to include it explicitly. The models expressed in Eulerian coordinates use either an advective flux as described by Rommelaere et al. (1997), or use boxes of air that are shifted downwards at regular time intervals (Schwander et al., 1993). Convection (fourth column) is handled in two different ways. The LGGE-GIPSA model uses a D_{eddy} term that is tuned by the RMSD minimisation algorithm, in combination with zero gravitational fractionation for $z < 4$ m. The other models use the parameterisation of Kawamura et al. (2006) where a D_{eddy} term is included that falls off exponentially with depth. The fifth column of Table 1 indicates whether the time stepping used in solving the diffusion equation was either explicit (Euler forward), implicit (Euler backward) or mixed implicit-explicit (Crank-Nicolson method). Finally, some of the models were tuned through manual adjustments of the diffusivity profile, while others used an automated control method (e.g. Rommelaere et al., 1997; Trudinger et al., 2002).

3.3 Fit of modeled profiles to the data[*]

The modeled profiles for all 10 tracers from the EU borehole are shown in Fig. 3, profiles from the US borehole can be found in the Supplement.

For CO_2 (Fig. 3a) we find a pronounced mismatch for $z > 70$ m which is reproduced consistently by all models and in both boreholes. The atmospheric reconstruction is based on the Law Dome record (Etheridge et al., 1996), and consequently the largest source of uncertainty is the interhemispheric CO_2 gradient. To explain the observed mismatch with an error in the atmospheric history would require a 6 ppm interhemispheric gradient in the 1950s, which can be ruled out (Keeling et al., 2010). Also contamination with modern air can be ruled out for these flasks, based on measurements of halocarbons. We cannot, however, exclude in-situ production of CO_2 from e.g. organic material or (bi)carbonates found in Greenland ice (e.g. Tschumi and Stauffer, 2000). There might also be a small close-off fractionation of CO_2, of order 1‰ or less, based on its effective molecular diameter (Huber et al., 2006; Severinghaus and Battle, 2006).

Both CH_3CCl_3 and $^{14}CO_2$ (Fig. 3d–e) have a peak within the LIZ. The peak height and position, which are sensitive to the shape and magnitude of the diffusivity profile, provide an important constraint in the tuning procedure. It is exactly at these peaks that the divergence between the models is most easily visible. It must be noted, however, that equally large model differences are found for other tracers as well (e.g. CO_2 and HFC-134a). Furthermore, models that fit the peak height exactly do not necessarily provide the best overall fit to the data.

To quantitatively assess how well the modeled profiles fit the data, we make a histogram of $(m_i - d_i)/\sigma_i$ where the index i goes over all 204 data points of the EU borehole. The σ_i are the unique uncertainties we assigned to each data point. This is shown in Fig. 4 together with a Gaussian distribution of width $\sigma = 1$ and a surface area equal to that of the histogram. The figure furthermore shows the RMSD from the data as given by Eq. (3). For all models we find a distribution that is more narrow than the Gaussian distribution, meaning that within the assigned uncertainties all data from the borehole can be modeled consistently. It also indicates the uncertainty estimates were chosen conservatively. The good agreement gives confidence in the correctness of our reconstructed atmospheric histories, which will be of use in future firn air studies. For the US hole the RMSD ranges between 0.60–1.06.

4 Model intercomparison

4.1 Diffusivity profiles and gas age distributions[*]

All the models are tuned separately to optimise the fit to the data. Figure 5A shows the reconstructed molecular diffusivity profiles for CO_2. The spread between the solutions is caused by two factors. First, it reflects differences in model physics, which are compensated for by adjustments to the diffusivity profile. Second, it relates to the degree in which the inverse problem of diffusivity reconstruction is under-determined. By using 10 different tracers the problem is more strongly constrained than in the case of using only CO_2, but the solution is not unique.

A second important observation is that all models require a non-vanishing diffusivity on the order of $2 \times 10^{-9}\,\mathrm{m^2\,s^{-1}}$ within the LIZ (see Fig. 5b). This contradicts the notion that diffusivity vanishes completely in the LIZ due to the presence of impermeable layers, which is frequently expressed in firn air studies (e.g. Battle et al., 1996; Trudinger et al., 2002; Assonov et al., 2005). Our findings confirm a recent study at Megadunes, Antarctica, that also reports a finite (eddy) diffusivity in the LIZ (Severinghaus et al., 2010). We believe this result to be robust, since it is reproduced by all six firn air models. Especially the well reproduced height of the $^{14}CO_2$ bomb spike, which falls entirely within the LIZ, provides strong evidence for finite LIZ diffusion at NEEM; letting diffusivity go to zero leads to a $^{14}CO_2$ peak that is too narrow and overshoots the measured values by $\sim 7\sigma$.

How the LIZ diffusivity is parameterised, however, varies strongly among the models as shown in Fig. 5c. The models use either molecular diffusion, dispersion (eddy diffusion) or a mixture of both. To fit the $\delta^{15}N_2$ data, most models require (a certain degree of) dispersive mixing in the LIZ since molecular diffusion would lead to continued gravitational fractionation. The LGGE-GIPSA model circumvents this problem by using a combination of Fick's and Darcy's transport to describe almost-stagnant transport in the lower zones (Witrant et al., 2011), which allows for using purely molecular diffusion in the LIZ. The SIO model uses the ratio of eddy to molecular diffusion in the LIZ as a tuning parameter in the RMSD minimisation, and finds that the fit is optimised for 27 % eddy diffusion (Supplement). Models that reproduce the observations equally well can have completely different parameterisations, so our analysis does not tell us which scheme is more likely to be correct. These model differences do have important consequences for the modeling of isotopic ratios, as is discussed below.

Firn air does not have a single age, but rather a distribution of ages (Schwander, 1993). The modeled gas age distribution, also referred to as Green's function, transfer function, response function or age spectrum, provides a complete description of the model transport properties (Rommelaere et al., 1997). Figure 6 compares CO_2 age distribution densities for the models at the lock-in depth ($z = 63\,\mathrm{m}$) and at the bottom

of the LIZ ($z = 78$ m, close to the deepest EU hole sample at $z = 77.75$ m). The most relevant characteristics of the age distributions are summarised in Table 2.

The LIZ lies beteen the two depths depicted here. From the closed porosity parameterisation (Eq. 1), we find that ~ 95 % of the air is trapped in this zone. The gas age distribution found in NEEM ice below the full close-off depth ($s_{op} = 0$) will be intermediate to these two end members, with a tail of older air trapped already in the DZ. Interestingly, at the lock-in depth ($z = 63$ m) estimates of both the age and the distribution width show a spread of around 30 % between models that reproduce the data equally well. Clearly these properties are not as well determined as one would expect based on the similarity between the modeled curves alone. On traversing the LIZ to $z = 78$ m the absolute spread in the calculated mean ages grows only slightly to about 5 yr. The spread in the distribution width remains large, however.

For the US borehole the spread in the calculated mean ages is even larger, with up to 50 % spread between ages at $z = 63$ m. This is due to the fact that we have only 4 tracers on the US borehole, and therefore the mean ages are less strongly constrained by the data.

We can use the gas age distributions to calculate the NEEM modern day Δage, i.e. the difference between gas age and ice age below the firn-ice transition. From annual layer counting and matching of reference horizons to the NGRIP GICC05 timescale (Rasmussen et al., 2006), the ice at depth $z = 63$ (78) m is estimated to be 190.6 (252.5) $\pm$ 1 yr old (S. O. Rasmussen, personal communication, 2011). Calculating the true Δage we would require the gas age in the closed porosity. With the model results of Table 2 we can only calculate Δage_{op}, i.e. the difference between ice age and gas age in the open pores. By averaging results from the six firn air models we find a Δage_{op} of 181 and 183 yr at $z = 63$ and 78 m, respectively. Clearly the ice and the air age at the same rate in the LIZ. We estimate the uncertainty in the true Δage to be about 8 yr, which is the maximum error that can be introduced by the ~ 5 % air trapped at depths $z < 63$ m. Based on these considerations our best estimate of the true Δage is 182 $\pm$ 8 yr. For the US borehole we obtain a best estimate Δage of 181 yr.

Finally we compare the reconstructed diffusivity profiles and gas age distributions for the EU and US boreholes. Figure 7a shows the total diffusivity with depth for CO_2 on a semilog scale, where we have averaged over the solutions from the different firn air models. We observe that the largest divergence between the boreholes occurs in the LIZ. Also the gas age distributions show divergence mainly in the LIZ. Figure 7b shows the age distributions at two depths, where again the curves represent an average over model output from the different firn air models. At the lock-in depth ($z = 63$ m) the age distributions of both boreholes are still very similar. After traversing the LIZ ($z = 76$ m, chosen to be near the final sampling depth on the US hole), we find that the firn air in the US hole has undergone more diffusive mixing, leading to a broader distribution width.

Polar firn is a layered medium that exhibits density variations with depth caused by seasonal variations in local climatic conditions and deposited snow density (e.g. Hörhold et al., 2011). Snow drift and redeposition at the surface lead to lateral inhomogeneities in the firn stratigraphy. The borehole comparison suggests that firn air transport in the LIZ is very sensitive to these lateral variations, whereas transport in the DZ is not. This is not unexpected since the formation of the LIZ has been linked to the degree of layering (Landais et al., 2006). If the amplitude of density variations is sufficiently large, the high-density layers will reach the close-off density before the low-density layers do, thus creating sealing layers that impede vertical diffusion and prevent further gravitational fractionation of the gas mixture (Martinerie et al., 1992; Schwander et al., 1993; Sturrock et al., 2002). Earlier we presented evidence for finite vertical mixing in the LIZ despite the presence of such impeding layers. The amount of vertical mixing is expected to depend on the horizontal extent of the sealing layers, as well as the position of (micro)cracks and passageways. This could lead to a strong lateral variation in LIZ diffusion as observed. Note that such lateral processes cannot be represented adequately in one-dimensional transport models.

4.2 Synthetic diagnostic scenarios*

To diagnose model properties further we developed four synthetic scenarios that probe specific aspects of the model physics.

4.2.1 Scenario I: diffusive fractionation

For gas species whose atmospheric mixing ratios change over time, the disequilibrium in the firn leads to an isotopic fractionation with depth, even in the absence of changes in atmospheric isotopic composition (Trudinger et al., 1997). To simulate this we increased the atmospheric mixing ratio of CO_2 monotonically at a rate similar to the modern day increase, while keeping the surface isotopic ratio fixed at $\delta^{13}CO_2 = 0$. Because the $^{13}CO_2$ isotopologue has a lower diffusivity, it is transported less efficiently into the firn, leading to a depletion in $^{13}CO_2$ with depth.

Figure 8a shows the modeled isotopic signal with depth for the different models. Results in the DZ are consistent, however they diverge strongly once the LIZ is reached. This depends mainly on the ratio of eddy- to molecular diffusion used to describe transport at these depths. We explore the ramifications of this model discrepancy in Sect. 5.

4.2.2 Scenario II: attenuation of a sine wave with depth

In this scenario we force the models with a sinusoidal atmospheric variation in CO_2 that has a 15 yr period. Due to diffusive smoothing, the amplitude of the signal decreases with depth in the firn. For mathematical convenience we impose two separate atmospheric scenarios:

$$[C_1](t, z = 0) = 1 + \sin\left(2\pi t / 15\right)$$
$$[C_2](t, z = 0) = 1 + \cos\left(2\pi t / 15\right)$$

where t is the time in years. Note that both signals are attenuated to the same degree by the diffusive smoothing, and that the $\pi/2$ phase angle between them is preserved.

To get the signal amplitude with depth, we combine the scenarios in the following way:

$$|[C](t,z)| = \sqrt{([C_1](t,z) - 1)^2 + ([C_2](t,z) - 1)^2} \qquad (4)$$

The outcome is shown in Fig. 8b. We observe that signal attenuation in the LIZ is stronger than in the DZ. This is because transport in the DZ is efficient; the mean CO_2 age at the lock-in depth is around 9 yr, which is less than the period of the atmospheric oscillation. The mixing ratios in most of the DZ will be "in phase" with the atmospheric signal, giving little attenuation. By comparison, air in the LIZ is nearly stagnant. It takes around 70 yr to be transported over 15 m, corresponding to almost 5 periods of the sinusoid. As air of different ages (i.e. different phases of the atmospheric cycle) gets mixed, the signal amplitude is reduced.

4.2.3 Scenario III: balance of transport fluxes

The total gas flux is the sum of the advective, diffusive and convective fluxes. The depth profiles of atmospheric species are affected by the sum of these components; to compare their relative strength we now look at the gravitational enrichment with depth for a hypothetical gas X which has a very small diffusion coefficient $D_X^0 = 0.025 D_{CO_2}^0$ and mass $M_X = M_{air} + 1 \, \mathrm{g\,mol^{-1}}$. Figure 8c shows the resulting curves together with the true gravitational enrichment as measured for $^{15}N_2$. In thermodynamic equilibrium the enrichment is given by the barometric equation: $\delta_{grav}(z) = [\exp(\Delta M g z / RT) - 1] \approx \Delta M g z / RT$ (Sowers et al., 1992). The advective and convective fluxes drive the air column out of equilibrium reducing $\delta_{grav}(z)$ below the barometric case. For gas X the diffusive flux is not large enough to oppose the other two, leading to a final δ_{grav} which is about half that of $^{15}N_2$. In this way the enrichment with depth represents the balance between the transfer mechanisms.

The differences in implementation of the convective mixing are clearly visible. The LGGE-GIPSA model uses no gravitational enrichment in the top 4 m, while the other models do. The CSIRO model has a stronger advective term (see below), which is reflected in a more reduced slope.

4.2.4 Scenario IV: advection with the ice matrix

Bubble trapping removes air from the open pores, which is subsequently advected downwards with the ice matrix. A downward flux of air in the open pores compensates for this removal. In the last scenario we study hypothetical gas Y, which is not subject to diffusion or convection, and is transported into the firn by this advective flux alone. Both eddy and molecular diffusion are set to zero. Its atmospheric history is a linear decrease by 1 ppm yr^{-1}, until it reaches zero at the final model date. This leads to a mixing ratio of gas Y in the firn that equals the age of the air at each depth. The results are shown in Fig. 8d. In the absence of diffusion most models find an age of around 900 yr at the bottom of the firn column. Models with less numerical diffusion produce larger ages. Also differences in total air flux affect the advective transport, and thereby the modeled ages.

5 Discussion

We find large differences in the way advective transport is treated by the models. The key difference is whether or not the model includes an upward air flow relative to descending ice layers to account for compression of open pores (Rommelaere et al., 1997; Sugawara et al., 2003). This term is neglected in the CSIRO model (Trudinger et al., 1997), which leads to a gas age that equals the ice age in scenario IV. The other models do include the back flux, which means that in scenario IV the gases need more time (~900 yr) to reach the lock-in depth. Note that the observed difference is not related to the choice of reference frame (static vs. moving).

Neglecting the back flow term corresponds to a physical model of the firn where all the air is transported downwards with the ice layers. This would be possible if e.g. the denser firn layers succeed in completely sealing off the air below (Martinerie et al., 1992; Schwander et al., 1993). In the case such impermeable layers are present in the LIZ, pressure will build up in the pore space below. At some of the Law Dome sites (e.g. DSSW20K) outgassing was observed from freshly drilled boreholes, which could be caused by the venting of such pressurised pores to the atmosphere. However, at these sites effects of wind pumping could not be excluded as the origin of the observed air flow. At NEEM, no outgassing from pressurised pores was observed. More evidence for the absence of impermeable layers comes from the observation of diffusive mixing in the LIZ, as discussed above. Furthermore, the total air content implied by the assumption of fully pressurised pores in the LIZ is incompatible with observed air content in mature ice (Martinerie et al., 1992).

For these reasons we believe that at the NEEM site the back flow due to pore compression can not be neglected when describing the firn air transport. This makes the assumptions in the CSIRO model less valid, explaining why it obtains a higher RMSD than the other models (Fig. 4). Preliminary tests show that by including the advective back flux in the CSIRO model the RMSD reduces to 0.74 (Trudinger et al., 2011). The OSU model also obtains a higher RMSD than most other models, despite the fact that it does incorporate the back flow term. We attribute this to the OSU tuning procedure for the molecular diffusivity profile, which has fewer degrees of freedom than the procedures used by the other models (Supplement).

The reference tracers used in the tuning procedure are sensitive to the total transport flux, which is the sum of the diffusive and advective terms. A higher advective flux can partially be compensated by a lower diffusivity, and vice versa. This explains why the diffusivity profile reconstructed through the CSIRO model is slightly lower than those of the other models (see Fig. 5a). In scenario III the balance between advective and diffusive mass transfer is visible as the slope of the gravitational enrichment with depth. The different amounts of advection lead to a difference in slope, in line with expectation.

In the LIZ transport is dominated by advection, so this is where we expect to find the largest differences between the two assumptions. Indeed we see that the LIZ is where the total diffusivity (Fig. 5b) and diffusive smoothing (Fig. 8b) diverge most strongly.

Scenarios II–IV are instructive in exposing differences in model physics, but the results have little consequences for realistic cases where the models agree well with each other and with the data (Fig. 3). Scenario I, on the other hand, is very realistic and the model divergence observed there is of greater concern. As a scenario we used a monotonic CO_2 increase of $\sim$1 ppm yr^{-1} without seasonal cycle, chosen to resemble the current anthropogenic increase (Keeling et al., 2010). Ice core and firn air records need to be corrected for the effect of diffusive fractionation (DF). For example, the corrections for the recent anthropogenic increase found in literature are $\sim$0.1‰ for $\delta^{13}CO_2$, and 1.2‰ for $\delta^{13}CH_4$ (Francey et al., 1999; Mischler et al., 2009).

The observed range between the different model solutions in the deepest firn is 0.05‰, which is around 40% of the total DF signal. For isotopes of CH_4 the DF is larger, because of the larger relative mass difference between the isotopologues. Based on the observed DF model disagreement we estimate an uncertainty of 0.5‰ for both $\delta^{13}C$ and δD of CH_4. For δD of CH_4 this uncertainty is smaller than the typical measurement uncertainty, as well as the atmospheric signal observed in the firn (Bräunlich et al., 2001; Mischler et al., 2009). However, for both $\delta^{13}CO_2$ and $\delta^{13}CH_4$ the model disagreement exceeds the typical instrumental precision. At this moment we have no objective way of determining which of the models predicts the DF correctly. This additional uncertainty should therefore be recognised when interpreting ice core and firn gas isotopic records of periods with rapid atmospheric variations. Sites with a thick LIZ combined with a low accumulation rate allow for reconstructing atmospheric mixing ratios further back in time. However, a thick LIZ also means a larger uncertainty in DF (and thereby isotopic reconstruction) due to the poorly constrained LIZ transport.

Molecular diffusion leads to DF between isotopologues because their diffusion coefficients are different. Advection, convection and dispersion do not discriminate between isotopologues, and consequently do not fractionate the gas mixture. The observed

model disagreement originates in the way in which LIZ transport is parameterised (Fig. 5c). The CIC and OSU models both smoothly go from purely molecular diffusion in the DZ to purely eddy diffusion in the LIZ. Once the molecular diffusion reaches zero, the DF ceases to increase with depth giving a horizontal line. The LGGE-GIPSA model on the other hand uses molecular diffusion all the way down to the close-off depth, giving a continued fractionation with depth. One way the DF uncertainty could be incorporated in future studies is by testing different parameterisations for LIZ diffusion, or by using transfer functions generated by different models.

The Law Dome-based records of $\delta^{13}CO_2$ (Francey et al., 1999) and $\delta^{13}CH_4$ (Ferretti et al., 2005) were both corrected for the effects of DF. The correction should not be affected much by our findings here for several reasons. Most importantly, the accumulation rate (and therefore the advective flux) at the Law Dome DSS, DE08 and DE08-2 sites is very large. This will strongly reduce DF in the LIZ as described above. Furthermore the LIZ is relatively thin (Trudinger, 2001). The study by Ferretti et al. (2005) combines ice core samples from the abovementioned high accumulation Law Dome sites with firn air measurements from the DSSW20K site, which has a rather low accumulation rate ($\sim 0.16\,\mathrm{m\,yr^{-1}}$ ice equivalent). After DF correction the results agree well. In other published firn air and ice core isotopic records that cover the recent anthropogenic increase (e.g. Bräunlich et al., 2001; Sugawara et al., 2003; Röckmann et al., 2003; Sowers et al., 2005; Bernard et al., 2006; Ishijima et al., 2007; Mischler et al., 2009) the uncertainty in the reconstruction due to the DF correction might have been underestimated.

6 Summary and conclusions

We presented a new multi-tracer method for characterising the firn air transport properties of a site. We applied the method to NEEM, Northern Greenland, by tuning six firn air models to an ensemble of ten tracers. The firn air models used in this study were able to fit the data within a 1-σ normal distribution, meaning that the site can be modeled consistently within the estimated uncertainties. Each of the reference tracers

constrains the firn profile differently through its unique atmospheric history and free air diffusivity, making our multiple-tracer characterisation method an improvement over the commonly used single-tracer tuning.

Six different firn air transport models were tuned to the NEEM site in this fashion, allowing a direct model comparison. We find that all the models require a non-vanishing diffusivity in the lock-in zone to reproduce the measured profiles of the reference gases. This is contrary to the commonly held notion that diffusive mixing is absent in the lock-in zone. A comparison between two boreholes located 64 m apart suggests that this lock-in zone diffusion is sensitive to lateral inhomogeneities in firn stratigraphy. Furthermore, we find that despite the fact that the models reproduce the measured profiles equally well, the gas age distributions they calculate can differ substantially. Often-used quantities, such as the mean age and distribution width, differed among the models by up to 30 %. The modern day Δage was calculated to be 182 ± 8 yr.

Finally we introduced four diagnostic scenarios that are designed to probe specific aspects of the model physics, from which we can draw two main conclusions. First, there are major differences in the way the models handle advective transport. The CSIRO model advects gases downward at the same velocity as the ice matrix, corresponding to a firn column with impermeable layers in the lock-in zone that can build up pressure below. The other models include a backflow of air relative to the descending ice layers, which corresponds to a situation without such layers and barometric equilibrium with the overlying atmosphere. Second, we find that the effect of isotopic diffusive fractionation is poorly constrained by the models. Near the close-off depth the calculated diffusive fractionation differs by 40 % between the models. These differences are related to the way in which lock-in zone diffusion is parameterised. Molecular diffusion leads to continued fractionation, whereas dispersion (eddy diffusion) does not. Further work is needed to elucidate the true nature of lock-in zone diffusion. Meanwhile, when interpreting firn air and ice core isotopic records an additional uncertainty needs to be included to account for the model discrepancy found here.

Supplementary material related to this article is available online at:
http://www.atmos-chem-phys-discuss.net/11/15975/2011/
acpd-11-15975-2011-supplement.zip.

Title Page

Abstract	Introduction
Conclusions	References
Tables	Figures

|◄ | ►|
◄ | ►

Back | Close

Full Screen / Esc

Printer-friendly Version

Interactive Discussion

References

Arnaud, L., Barnola, J. M., and Duval, P.: Physical modeling of the densification of snow/firn and ice in the upper part of polar ice sheets, in: Physics of Ice Core Records, edited by Hondoh, T., 285–305, Hokkaido University Press, 2000. 15981

Assonov, S. S., Brenninkmeijer, C. A. M., and Jockel, P.: The O-18 isotope exchange rate between firn air CO_2 and the firn matrix at three Antarctic sites, J. Geophys. Res.-Atmos., 110(15), D18310, doi:10.1029/2005jd005769, 2005. 15992

Assonov, S. S., Brenninkmeijer, C. A. M., Jöckel, P., Mulvaney, R., Bernard, S., and Chappellaz, J.: Evidence for a CO increase in the SH during the 20th century based on firn air samples from Berkner Island, Antarctica, Atmos. Chem. Phys., 7, 295–308, doi:10.5194/acp-7-295-2007, 2007. 15978

Aydin, M., Saltzman, E. S., De Bruyn, W. J., Montzka, S. A., Butler, J. H., and Battle, M.: Atmospheric variability of methyl chloride during the last 300 years from an Antarctic ice core and firn air, Geophys. Res. Lett., 31(4), L02109, doi:10.1029/2003gl018750, 2004. 15978

Battle, M., Bender, M., Sowers, T., Tans, P. P., Butler, J. H., Elkins, J. W., Ellis, J. T., Conway, T., Zhang, N., Lang, P., and Clarket, A. D.: Atmospheric gas concentrations over the past century measured in air from firn at the South Pole, Nature, 383, 231–235, doi:10.1038/383231a0, 1996. 15978, 15981, 15992

Bernard, S., Röckmann, T., Kaiser, J., Barnola, J.-M., Fischer, H., Blunier, T., and Chappellaz, J.: Constraints on N_2O budget changes since pre-industrial time from new firn air and ice core isotope measurements, Atmos. Chem. Phys., 6, 493–503, doi:10.5194/acp-6-493-2006, 2006. 15978, 16000

Bräunlich, M., Aballanin, O., Marik, T., Jockel, P., Brenninkmeijer, C. A. M., Chappellaz, J., Barnola, J. M., Mulvaney, R., and Sturges, W. T.: Changes in the global atmospheric methane budget over the last decades inferred from C-13 and D isotopic analysis of Antarctic firn air, J. Geophys. Res.-Atmos., 106, 20465–20481, doi:10.1029/2001JD900190, 2001. 15999, 16000

Butler, J. H., Battle, M., Bender, M. L., Montzka, S. A., Clarke, A. D., Saltzman, E. S., Sucher, C. M., Severinghaus, J. P., and Elkins, J. W.: A record of atmospheric halocarbons during the twentieth century from polar firn air, Nature, 399, 749–755, 1999. 15978

Chen, N. H. and Othmer, D. F.: New Generalized Equation for Gas Diffusion Coefficient, J. Chem. Eng. Data, 7, 37–41, 1962. 15988

Title Page

Abstract | Introduction

Conclusions | References

Tables | Figures

◄◄ | ►►

◄ | ►

Back | Close

Full Screen / Esc

Printer-friendly Version

Interactive Discussion

Colbeck, S. C.: Air movement in snow due to windpumping, J. Glaciol., 35, 209–213, 1989. 15988

Conway, T. J., Tans, P. P., Waterman, S., L., and Thoning, K. W.: Evidence for interannual variability of the carbon-cycle from the National-Oceanic-and-Atmospheric-Administration Climate-Monitoring-and-Diagnostics-Laboratory Global-air-sampling-network, J. Geophys. Res.-Atmos., 99, 22831–22855, 1994. 15983, 15984

Craig, H., Horibe, Y., and Sowers, T.: Gravitational Separation of Gases and Isotopes in Polar Ice Caps, Science, 242, 1675–1678, 1988. 15978, 15985

Cunnold, D., Weiss, R., Prinn, R., Hartley, D., Simmonds, P., Fraser, P., Miller, B., Alyea, F., and Porter, L.: GAGE/AGAGE measurements indicating reductions in global emissions of CCl_3F and CCl_2F_2 in 1992–1994, J. Geophys. Res.-Atmos., 102, 1259–1269, doi:10.1029/96JD02973, 1997. 15984

Dlugokencky, E. J., Steele, L. P., Lang, P. M., and Masarie, K. A.: The growth-rate and distribution of atmospheric methane, J. Geophys. Res.-Atmos., 99, 17021–17043, 1994. 15983, 15984

Dreyfus, G. B., Jouzel, J., Bender, M. L., Landais, A., Masson-Delmotte, V., and Leuenberger, M.: Firn processes and $\delta^{15}N$: potential for a gas-phase climate proxy, Quaternary Sci. Rev., 29, 28–42, doi:10.1016/j.quascirev.2009.10.012, 2010. 15979

Etheridge, D. M., Steele, L. P., Langenfelds, R. L., Francey, R. J., Barnola, J. M., and Morgan, V. I.: Natural and anthropogenic changes in atmospheric CO_2 over the last 1000 years from air in Antarctic ice and firn, J. Geophys. Res., 101, 4115–4128, doi:10.1029/95JD03410, 1996. 15985, 15990

Etheridge, D. M., Steele, L., Francey, R., and Langenfelds, R.: Atmospheric methane between 1000 AD and present: Evidence of anthropogenic emissions and climatic variability, J. Geophys. Res.-Atmos., 103, 15979–15993, doi:10.1029/98JD00923, 1998. 15978, 15985

Fabre, A., Barnola, J. M., Arnaud, L., and Chappellaz, J.: Determination of gas diffusivity in polar firn: Comparison between experimental measurements and inverse modeling, Geophys. Res. Lett., 27, 557–560, doi:10.1029/1999GL010780, 2000. 15979

Ferretti, D. F., Miller, J. B., White, J. W. C., Etheridge, D. M., Lassey, K. R., Lowe, D. C., Meure, C. M. M., Dreier, M. F., Trudinger, C. M., van Ommen, T. D., and Langenfelds, R. L.: Unexpected changes to the global methane budget over the past 2000 years, Science, 309, 1714–1717, doi:10.1126/science.1115193, 2005. 15978, 16000

Francey, R., Allison, C., Etheridge, D., Trudinger, C., Enting, I., Leuenberger, M., Langenfelds,

R., Michel, E., and Steele, L.: A 1000-year high precision record of delta C-13 in atmospheric CO_2, Tellus B, 51, 170–193, doi:10.1034/j.1600-0889.1999.t01-1-00005.x, 1999. 15978, 15984, 15985, 15999, 16000

Francey, R. J., Steele, L. P., Spencer, D. A., Langenfelds, R. L., Law, R. M., Krummel, P. B., Fraser, P. J., Etheridge, D. M., Derek, N., Coram, S. A., Coopen, L. N., Allison, C. E., Porter, L., and Baly, S.: The CSIRO (Australia) measurement of greenhouse gases in the global atmosphere, in: Baseline Atmospheric Program Australia 1999–2000, edited by: Tindale, N. W., Derek, N., and Fraser, P. J., 42–53, Bureau of Meteorology, Melbourne, Victoria, Australia, 2003. 15983, 15984

Fraser, P., Cunnold, D., Alyea, F., Weiss, R., Prinn, R., Simmonds, P., Miller, B., and Langenfelds, R.: Lifetime and emission estimates of 1,1,2-trichlorotrifluorethane (CFC-113) from daily global background observations June 1982 June 1994, J. Geophys. Res.-Atmos., 101, 12585–12599, doi:10.1029/96JD00574, 1996. 15984

Geller, L., Elkins, J., Lobert, J., Clarke, A., Hurst, D., Butler, J., and Myers, R.: Tropospheric SF_6: Observed latitudinal distribution and trends, derived emissions and interhemispheric exchange time, Geophys. Res. Lett., 24, 675–678, doi:10.1029/97GL00523, 1997. 15984

Goujon, C., Barnola, J. M., and Ritz, C.: Modeling the densification of polar firn including heat diffusion: Application to close-off characteristics and gas isotopic fractionation for Antarctica and Greenland sites, J. Geophys. Res.-Atmos., 108(18), 4792, doi:10.1029/2002jd003319, 2003. 15982

Hörhold, M. W., Kipfstuhl, S., Wilhelms, F., Freitag, J., and Frenzel, A.: The densification of layered polar firn, J. Geophys. Res.-Earth., 116, F01001, doi:10.1029/2009JF001630, 2011. 15994

Huber, C., Beyerle, U., Leuenberger, M., Schwander, J., Kipfer, R., Spahni, R., Severinghaus, J. P., and Weiler, K.: Evidence for molecular size dependent gas fractionation in firn air derived from noble gases, oxygen, and nitrogen measurements, Earth Planet. Sci. Lett., 243, 61–73, doi:10.1016/j.epsl.2005.12.036, 2006. 15978, 15986, 15990

Ishijima, K., Sugawara, S., Kawamura, K., Hashida, G., Morimoto, S., Murayama, S., Aoki, S., and Nakazawa, T.: Temporal variations of the atmospheric nitrous oxide concentration and its delta N-15 and delta O-18 for the latter half of the 20th century reconstructed from firn air analyses, J. Geophys. Res.-Atmos., 112(12), D03305, doi:10.1029/2006jd007208, 2007. 15978, 16000

Kawamura, K., Severinghaus, J. P., Ishidoya, S., Sugawara, S., Hashida, G., Motoyama, H.,

Fujii, Y., Aoki, S., and Nakazawa, T.: Convective mixing of air in firn at four polar sites, Earth Planet. Sci. Lett., 244, 672–682, doi:10.1016/j.epsl.2006.02.017, 2006. 15982, 15988, 15990

Kawamura, K., Parrenin, F., Lisiecki, L., Uemura, R., Vimeux, F., Severinghaus, J. P., Hutterli, M. A., Nakazawa, T., Aoki, S., Jouzel, J., Raymo, M. E., Matsumoto, K., Nakata, H., Motoyama, H., Fujita, S., Goto-Azuma, K., Fujii, Y., and Watanabe, O.: Northern Hemisphere forcing of climatic cycles in Antarctica over the past 360,000 years, Nature, 448, 912–916, doi:10.1038/nature06015, 2007. 15979

Keeling, C. D., Piper, S. C., Whorf, T. P., and Keeling, R. F.: Evolution of natural and anthropogenic fluxes of atmospheric CO_2 from 1957 to 2003, Tellus B, 63, 1–22, doi:10.1111/j.1600-0889.2010.00507.x, 2010. 15990, 15999

Keeling, R. F., Piper, S. C., Bollenbacher, A. F., and Walker, J. S.: Atmospheric CO_2 records from sites in the SIO air sampling network, in: Trends: A Compendium of Data on Global Change, Carbon Dioxide Information Analysis Center, Oak Ridge National Laboratory, U.S. Department of Energy, Oak Ridge, Tenn., USA, 2009. 15984

Landais, A., Caillon, N., Goujon, C., Grachev, A. M., Barnola, J. M., Chappellaz, J., Jouzel, J., Masson-Delmotte, V., and Leuenberger, M.: Quantification of rapid temperature change during DO event 12 and phasing with methane inferred from air isotopic measurements, Earth Planet. Sci. Lett., 225, 221–232, doi:10.1016/j.epsl.2004.06.009, 2004. 15979

Landais, A., Barnola, J. M., Kawamura, K., Caillon, N., Delmotte, M., Van Ommen, T., Dreyfus, G., Jouzel, J., Masson-Delmotte, V., Minster, B., Freitag, J., Leuenberger, M., Schwander, J., Huber, C., Etheridge, D., and Morgan, V.: Firn-air delta N-15 in modern polar sites and glacial-interglacial ice: a model-data mismatch during glacial periods in Antarctica?, Quaternary Sci. Rev., 25, 49–62, 2006. 15994

Laube, J. C., Martinerie, P., Witrant, E., Blunier, T., Schwander, J., Brenninkmeijer, C. A. M., Schuck, T. J., Bolder, M., Röckmann, T., van der Veen, C., Bönisch, H., Engel, A., Mills, G. P., Newland, M. J., Oram, D. E., Reeves, C. E., and Sturges, W. T.: Accelerating growth of HFC-227ea (1,1,1,2,3,3,3-heptafluoropropane) in the atmosphere, Atmos. Chem. Phys., 10, 5903–5910, doi:10.5194/acp-10-5903-2010, 2010. 15983

Levin, I. and Kromer, B.: The tropospheric (CO_2)-C-14 level in mid-latitudes of the Northern Hemisphere (1959–2003), Radiocarbon, 46, 1261–1272, 2004. 15984

Levin, I., Hammer, S., Kromer, B., and Meinhardt, F.: Radiocarbon observations in atmospheric CO_2: Determining fossil fuel CO_2 over Europe using Jungfraujoch observations as back-

Title Page

Abstract | Introduction

Conclusions | References

Tables | Figures

◄ | ►

◄ | ►

Back | Close

Full Screen / Esc

Printer-friendly Version

Interactive Discussion

ground, Sci. Total Environ., 391, 211–216, doi:10.1016/j.scitotenv.2007.10.019, 2008. 15984

Levin, I., Naegler, T., Heinz, R., Osusko, D., Cuevas, E., Engel, A., Ilmberger, J., Langenfelds, R. L., Neininger, B., Rohden, C. v., Steele, L. P., Weller, R., Worthy, D. E., and Zimov, S. A.: The global SF6 source inferred from long-term high precision atmospheric measurements and its comparison with emission inventories, Atmos. Chem. Phys., 10, 2655–2662, doi:10.5194/acp-10-2655-2010, 2010. 15983

Levin, I., Hammer, S., Eichelmann, E., and Vogel, F.: Verification of greenhouse gas emission reductions: The prospect of atmospheric monitoring in polluted areas, Philos. T. Roy. Soc. A, 369, 1906–1924, 2011. 15983

MacFarling Meure, C., Etheridge, D., Trudinger, C., Steele, P., Langenfelds, R., van Ommen, T., Smith, A., and Elkins, J.: Law Dome CO_2, CH_4 and N_2O ice core records extended to 2000 years BP, Geophys. Res. Lett., 33, L14810 doi:10.1029/2006gl026152, 2006. 15985

Manning, M. and Melhuish, W. H.: Atmospheric Delta 14C record from Wellington, in: Trends: A Compendium of Data on Global Change, Carbon Dioxide Information Analysis Center, Oak Ridge National Laboratory, U.S. Department of Energy, Oak Ridge, Tenn., USA, 1994. 15984

Martinerie, P., Raynaud, D., Etheridge, D. M., Barnola, J. M., and Mazaudier, D.: Physical and climatic parameters which influence the air content in polar ice, Earth Planet. Sci. Lett., 112, 1–13, doi:10.1016/0012-821X(92)90002-D, 1992. 15994, 15998

Martinerie, P., Nourtier-Mazauric, E., Barnola, J.-M., Sturges, W. T., Worton, D. R., Atlas, E., Gohar, L. K., Shine, K. P., and Brasseur, G. P.: Long-lived halocarbon trends and budgets from atmospheric chemistry modelling constrained with measurements in polar firn, Atmos. Chem. Phys., 9, 3911–3934, doi:10.5194/acp-9-3911-2009, 2009. 15978, 15985

Matsunaga, N., Hori, M., and Nagashima, A.: Mutual diffusion coefficients of halogenated-hydrocarbon refrigerant-air systems, High Temp.-High Press., 25, 185–192, 1993. 15988

Matsunaga, N., Hori, M., and Nagashima, A.: Diffusion coefficients of global warming gases into air and its component gases, High Temp.-High Press., 30, 77–83, 1998. 15988

Matsunaga, N., Hori, M., and Nagashima, A.: Measurements of the mutual diffusion coefficients of gases by the Taylor method (7th Report, measurements on the SF_6-air, SF_6-N_2, SF_6-O_2, CFC12-N_2, CFC12-O_2, HCFC22-N_2 and HCFC22-O_2 systems), Trans. Jpn. Soc. Mech. Eng. B., 68, 550–555, 2002a. 15988

Matsunaga, N., Hori, M., and Nagashima, A.: Measurements of the mutual diffusion coefficients of gases by the Taylor method (8th Report, measurements on the HFC32-air, HCFC124-air,

Gas transport in firn: multiple-tracer characterisation for NEEM

C. Buizert et al.

Title Page

Abstract	Introduction
Conclusions	References
Tables	Figures

◀◀   ▶▶

◀   ▶

Back   Close

Full Screen / Esc

Printer-friendly Version

Interactive Discussion

HCFC125-air, HCFC143a-air, and HFC43-10mee-air systems), Trans. Jpn. Soc. Mech. Eng. B., 68, 550–555, 2002b. 15988

Mischler, J. A., Sowers, T. A., Alley, R. B., Battle, M., McConnell, J. R., Mitchell, L., Popp, T., Sofen, E., and Spencer, M. K.: Carbon and hydrogen isotopic composition of methane over the last 1000 years, Global Biogeochem. Cy., 23, GB4024, doi:10.1029/2009GB003460, 2009. 15999, 16000

Montzka, S., Myers, R., Butler, J., Elkins, J., Lock, L., Clarke, A., and Goldstein, A.: Observations of HFC-134a in the remote troposphere, Geophys. Res. Lett., 23, 169–172, doi:10.1029/95GL03590, 1996. 15984

Montzka, S. A., Aydin, M., Battle, M., Butler, J. H., Saltzman, E. S., Hall, B. D., Clarke, A. D., Mondeel, D., and Elkins, J. W.: A 350-year atmospheric history for carbonyl sulfide inferred from Antarctic firn air and air trapped in ice, J. Geophys. Res.-Atmos., 109(11), D22302, doi:10.1029/2004JD004686, 2004. 15978

Nydal, R. and Lövseth, K.: Carbon-14 Measurements in Atmospheric CO_2 from Northern and Southern Hemisphere Sites, 1962-1993, Carbon Dioxide Information Analysis Center, Oak Ridge National Laboratory, Oak Ridge, Tennessee, 1996. 15984

Prinn, R., Weiss, R., Fraser, P., Simmonds, P., Cunnold, D., Alyea, F., O'Doherty, S., Salameh, P., Miller, B., Huang, J., Wang, R., Hartley, D., Harth, C., Steele, L., Sturrock, G., Midgley, P., and McCulloch, A.: A history of chemically and radiatively important gases in air deduced from ALE/GAGE/AGAGE, J. Geophys. Res.-Atmos., 105, 17751–17792, doi:10.1029/2000JD900141, 2000. 15984

Prinn, R., Huang, J., Weiss, R., Cunnold, D., Fraser, P., Simmonds, P., McCulloch, A., Harth, C., Reimann, S., Salameh, P., O'Doherty, S., Wang, R., Porter, L., Miller, B., and Krummel, P.: Evidence for variability of atmospheric hydroxyl radicals over the past quarter century, Geophys. Res. Lett., 32, L07809, doi:10.1029/2004GL022228, 2005. 15984

Rasmussen, S., Andersen, K., Svensson, A., Steffensen, J., Vinther, B., Clausen, H., Siggaard-Andersen, M., Johnsen, S., Larsen, L., Dahl-Jensen, D., Bigler, M., Rothlisberger, R., Fischer, H., Goto-Azuma, K., Hansson, M., and Ruth, U.: A new Greenland ice core chronology for the last glacial termination, J. Geophys. Res.-Atmos., 111, D06102, doi:10.1029/2005JD006079, 2006. 15993

Reimer, P., Baillie, M., Bard, E., Bayliss, A., Beck, J., Bertrand, C., Blackwell, P., Buck, C., Burr, G., Cutler, K., Damon, P., Edwards, R., Fairbanks, R., Friedrich, M., Guilderson, T., Hogg, A., Hughen, K., Kromer, B., McCormac, G., Manning, S., Ramsey, C., Reimer, R., Remmele,

S., Southon, J., Stuiver, M., Talamo, S., Taylor, F., van der Plicht, J., and Weyhenmeyer, C.: IntCal04 terrestrial radiocarbon age calibration, 0-26 cal kyr BP, Radiocarbon, 46, 1029–1058, 2004. 15985

Röckmann, T., Kaiser, J., and Brenninkmeijer, C. A. M.: The isotopic fingerprint of the pre-industrial and the anthropogenic N_2O source, Atmos. Chem. Phys., 3, 315–323, doi:10.5194/acp-3-315-2003, 2003. 15978, 16000

Rommelaere, V., Arnaud, L., and Barnola, J. M.: Reconstructing recent atmospheric trace gas concentrations from polar firn and bubbly ice data by inverse methods, J. Geophys. Res.-Atmos., 102, 30069–30083, doi:10.1029/97JD02653, 1997. 15979, 15987, 15988, 15990, 15992, 15997

Schwander, J.: The transformation of snow to ice and the occlusion of gases, in: The Environmental record in glaciers and ice sheets, edited by: Oescher, H. and Langway, C., 53–67, John Wiley, New York, 1989. 15978, 15985, 15988

Schwander, J., Stauffer, B., and Sigg, A.: Air mixing in firn and the age of the air at pore close-off, Ann. Glaciol., 10, 141–145, 1988. 15987

Schwander, J., Barnola, J. M., Andrie, C., Leuenberger, M., Ludin, A., Raynaud, D., and Stauffer, B.: The age of the air in the firn and the ice at Summit, Greenland, J. Geophys. Res.-Atmos., 98, 2831–2838, 1993. 15978, 15981, 15990, 15992, 15994, 15998

Schwander, J., Sowers, T., Barnola, J. M., Blunier, T., Fuchs, A., and Malaize, B.: Age scale of the air in the summit ice: Implication for glacial-interglacial temperature change, J. Geophys. Res.-Atmos., 102, 19483–19493, doi:10.1029/97JD01309, 1997. 15978, 15982

Severinghaus, J. P. and Battle, M. O.: Fractionation of gases in polar lee during bubble close-off: New constraints from firn air Ne, Kr and Xe observations, Earth Planet. Sci. Lett., 244, 474–500, doi:10.1016/j.epsl.2006.01.032, 2006. 15978, 15986, 15989, 15990

Severinghaus, J. P. and Brook, E. J.: Abrupt climate change at the end of the last glacial period inferred from trapped air in polar ice, Science, 286, 930–934, doi:10.1126/science.286.5441.930, 1999. 15978

Severinghaus, J. P., Grachev, A., and Battle, M.: Thermal fractionation of air in polar firn by seasonal temperature gradients, Geochem. Geophy. Geosy., 2, 1048, doi:10.1029/2000GC000146, 2001. 15978, 15988, 16014

Severinghaus, J. P., Grachev, A., Luz, B., and Caillon, N.: A method for precise measurement of argon 40/36 and krypton/argon ratios in trapped air in polar ice with applications to past firn thickness and abrupt climate change in Greenland and at Siple Dome, Antarctica, Geochim.

Gas transport in firn: multiple-tracer characterisation for NEEM

C. Buizert et al.

Title Page

Abstract	Introduction
Conclusions	References
Tables	Figures

◄◄ ►►

◄ ►

Back Close

Full Screen / Esc

Printer-friendly Version

Interactive Discussion

Cosmochim. Ac., 67, 325–343, doi:10.1016/S0016-7037(02)00965-1, 2003. 15983

Severinghaus, J. P., Albert, M. R., Courville, Z. R., Fahnestock, M. A., Kawamura, K., Montzka, S. A., Muhle, J., Scambos, T. A., Shields, E., Shuman, C. A., Suwa, M., Tans, P., and Weiss, R. F.: Deep air convection in the firn at a zero-accumulation site, central Antarctica, Earth Planet. Sci. Lett., 293, 359–367, doi:10.1016/j.epsl.2010.03.003, 2010. 15992

Smith, A. M., Levchenko, V. A., Etheridge, D. M., Lowe, D. C., Hua, Q., Trudinger, C. M., Zoppi, U., and Elcheikh, A.: In search of in-situ radiocarbon in Law Dome ice and firn, in: 8th International Conference on Accelerator Mass Spectrometry, 610–622, Elsevier Science Bv, Vienna, Austria, 1999. 15983

Sowers, T., Bender, M., Raynaud, D., and Korotkevich, Y. S.: Delta-N-15 of N_2 in air trapped in polar ice - a tracer of gas-transport in the firn and a possible constraint on ice age-gas age-differences, J. Geophys. Res.-Atmos., 97, 15683–15697, 1992. 15982, 15985, 15996

Sowers, T., Bernard, S., Aballain, O., Chappellaz, J., Barnola, J., and Marik, T.: Records of the delta C-13 of atmospheric CH_4 over the last 2 centuries as recorded in Antarctic snow and ice, Global Biogeochem. Cy., 19, GB2002, doi:10.1029/2004GB002408, 2005. 16000

Spahni, R., Schwander, J., Flückiger, J., Stauffer, B., Chappellaz, J., and Raynaud, D.: The attenuation of fast atmospheric CH_4 variations recorded in polar ice cores, Geophys. Res. Lett., 30, 1571, doi:10.1029/2003GL017093, 2003. 15978

Stuiver, M. and Polach, H. A.: Reporting of C-14 data – discussion, Radiocarbon, 19, 355–363, 1977. 15984

Sturrock, G. A., Etheridge, D. M., Trudinger, C. M., Fraser, P. J., and Smith, A. M.: Atmospheric histories of halocarbons from analysis of Antarctic firn air: Major Montreal Protocol species, J. Geophys. Res.-Atmos., 107(14), 4765, doi:10.1029/2002JD002548, 2002. 15978, 15994

Sugawara, S., Kawamura, K., Aoki, S., Nakazawa, T., and Hashida, G.: Reconstruction of past variations of delta C-13 in atmospheric CO_2 from its vertical distribution observed in the firn at Dome Fuji, Antarctica, Tellus B, 55, 159–169, doi:10.1034/j.1600-0889.2003.00023.x, 2003. 15978, 15979, 15987, 15988, 15997, 16000

Trudinger, C.: The carbon cycle over the last 1000 years inferred from inversion of ice core data, Ph.D. thesis, 2001. 16000

Trudinger, C. M., Enting, I. G., Etheridge, D. M., Francey, R. J., Levchenko, V. A., Steele, L. P., Raynaud, D., and Arnaud, L.: Modeling air movement and bubble trapping in firn, J. Geophys. Res.-Atmos., 102, 6747–6763, doi:10.1029/96JD03382, 1997. 15978, 15979, 15988, 15989, 15995, 15997

Title Page

Abstract | Introduction

Conclusions | References

Tables | Figures

◀ | ▶

◀ | ▶

Back | Close

Full Screen / Esc

Printer-friendly Version

Interactive Discussion

Trudinger, C. M., Etheridge, D. M., Rayner, P. J., Enting, I. G., Sturrock, G. A., and Langenfelds, R. L.: Reconstructing atmospheric histories from measurements of air composition in firn, J. Geophys. Res.-Atmos., 107(13), 4780, doi:10.1029/2002JD002545, 2002. 15979, 15987, 15990, 15992, 16013

5 Trudinger, C. M., Etheridge, D. M., Sturrock, G. A., Fraser, P. J., Krummel, P. B., and McCulloch, A.: Atmospheric histories of halocarbons from analysis of Antarctic firn air: Methyl bromide, methyl chloride, chloroform, and dichloromethane, J. Geophys. Res.-Atmos., 109(15), D22310, doi:10.1029/2004JD004932, 2004. 15978, 15979

Trudinger, C. M., Enting, I. G., Rayner, P. J., Etheridge, D. M., Rubino, M., Buizert, C., Martinerie, P., Blunier, T.: How well do different tracers constrain the firn diffusivity profile?, in preparation, 2011.

Tschumi, J. and Stauffer, B.: Reconstructing past atmospheric CO_2 concentration based on ice-core analyses: open questions due to in situ production of CO_2 in the ice, J. Glaciol., 46, 45–53, 2000. 15986, 15990

15 Witrant, E., Martinerie, P., Severinghaus, J. P., Hogan, C., Laube, J. C., Kawamura, K., Capron, E., Montzka, S. A., Dlugokencky, E. J., Etheridge, D. M., Blunier, T., and Sturges, W. T.: A new multi-gas constrained model of trace gas non-homogeneous transport in firn: evaluation and behaviour at several polar sites, in preparation, 2011.

Table 1. Overview of firn air transport models. See text for explanation.

Model	Coordinates	Advection	Convection	Time stepping	Tuning
CIC	static	flux	exponential	Crank-Nic.	automated
CSIRO	moving	coordinates	exponential	Crank-Nic.	automated
INSTAAR	static	flux	exponential	explicit	manual
LGGE-GIPSA	static	flux	tuned	implicit	automated
OSU	static	boxes	exponential	Crank-Nic.	manual
SIO	static	boxes	exponential	explicit	automated
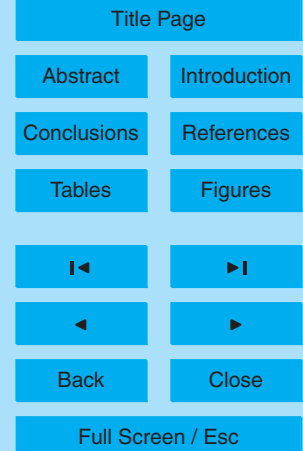
Table 2. Mean age, median age, Full Width at Half Maximum and Spectral Width (Δ, Eq. (1) in Trudinger et al., 2002) at the lock-in depth ($z = 63$ m) and at the bottom of the LIZ ($z = 78$ m). All values given in years.

Model	Mean	Median	FWHM	Δ
	$z = 63$ m			
CIC	9.4	7.6	7.9	4.5
CSIRO	10.5	9.0	9.3	4.2
INSTAAR	8.9	7.2	7.4	4.2
LGGE-GIPSA	11.3	8.3	9.1	6.8
OSU	8.1	6.7	7.0	3.7
SIO	9.2	7.4	7.6	4.5
	$z = 78$ m			
CIC	71.1	69.6	30.1	9.8
CSIRO	67.8	66.2	24.8	8.3
INSTAAR	68.5	66.3	37.1	12.4
LGGE-GIPSA	73.0	70.6	36.8	12.5
OSU	67.7	65.9	33.3	10.8
SIO	69.7	67.9	32.2	10.5
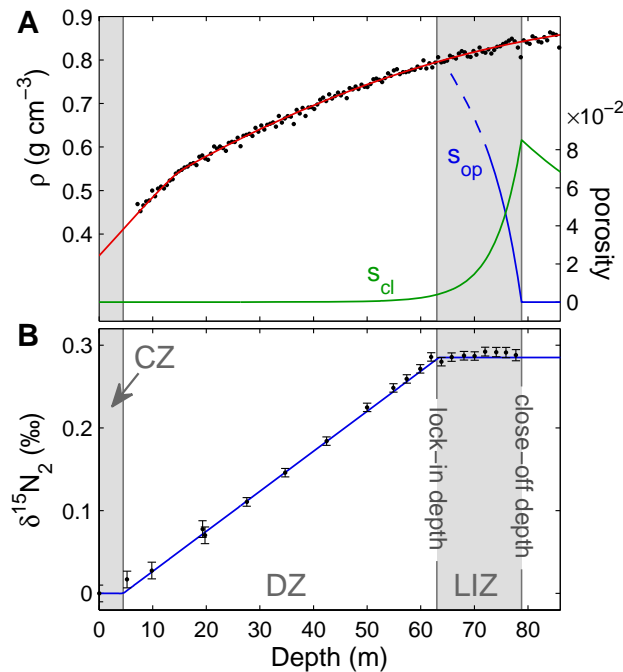
Fig. 1. (A) Firn density $\rho(z)$ (left axis), and the open and closed porosity s_{op} and s_{cl}, respectively (right axis). Black dots show firn density measurements in 0.55 m segments, the red line is the fit used in this study. **(B)** Gravitational enrichment as shown by $\delta^{15}N_2$, corrected for thermal effects (Severinghaus et al., 2001). The blue line shows the barometric slope $\Delta Mg(z-4.5)/RT$, where we use $\Delta M = 1 \times 10^{-3}\,\mathrm{kg\,mol^{-1}}$. Convective zone (CZ), diffusive zone (DZ) and lock-in zone (LIZ) are indicated by changes in shading.

ACPD

11, 15975–16021, 2011

Gas transport in firn: multiple-tracer characterisation for NEEM

C. Buizert et al.

Title Page

Abstract | Introduction

Conclusions | References

Tables | Figures

◀ | ▶|

◀ | ▶

Back | Close

Full Screen / Esc

Printer-friendly Version

Interactive Discussion
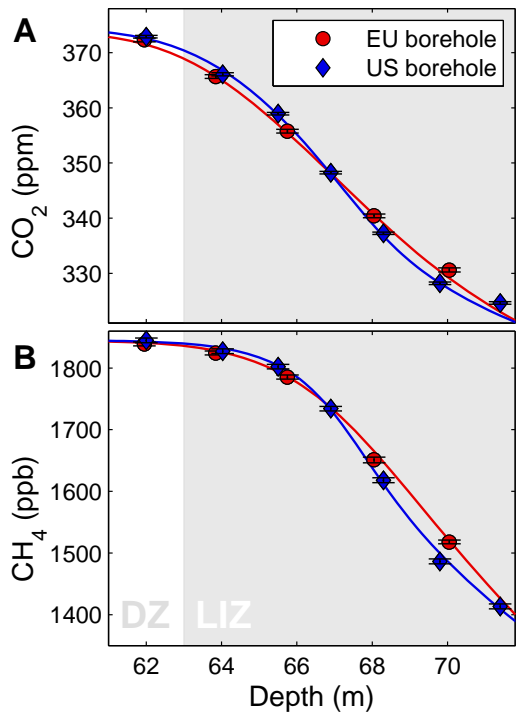
Fig. 2. Comparison of **(A)** CO_2 and **(B)** CH_4 data in the lock-in zone of the two boreholes. Data from three laboratories are averaged; the 1σ uncertainty bar is a combination of analytical and sampling uncertainties as specified in Sect. 2.7. Curves are modeled profiles using the CIC model, see Sect. 3.3.

Title Page

Abstract | Introduction

Conclusions | References

Tables | Figures

◄ | ►

◄ | ►

Back | Close

Full Screen / Esc

Printer-friendly Version

Interactive Discussion

Fig. 3. **(A–J)** Modeled profiles for all 10 tracers from the EU borehole. With the exception of **(J)** data is gravity corrected and the models are run with gravity turned off. Errorbars correspond to full 1σ uncertainty as defined in Sect. 2.7.
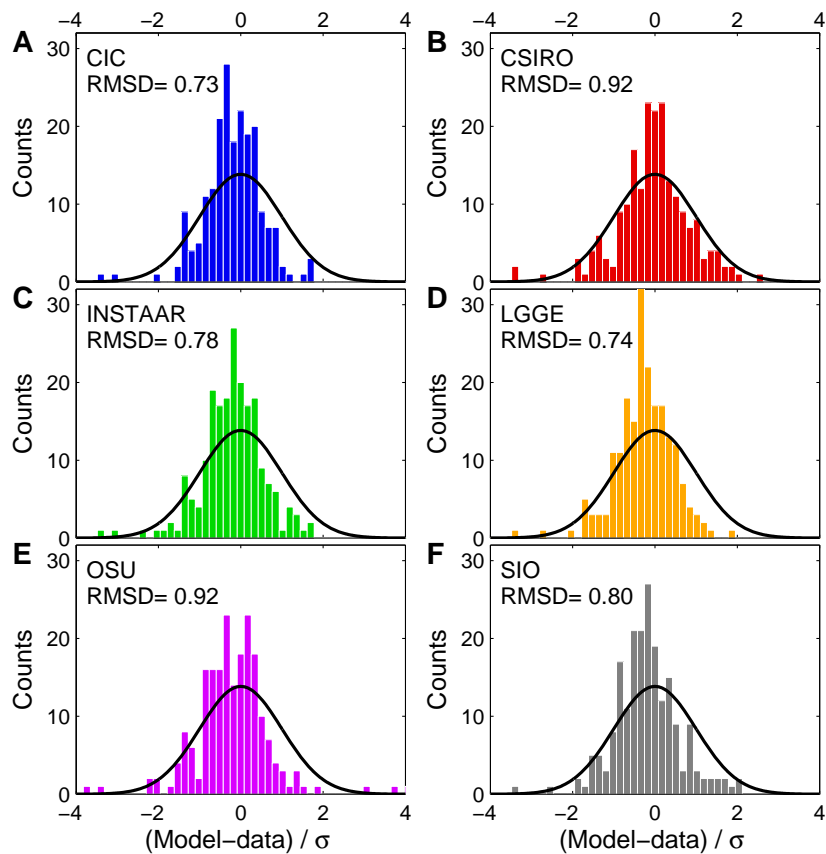
Fig. 4. (A–F) Histogram of $(m_i - d_i)/\sigma_i$ for the firn air transport models in this study using the EU borehole data. The black curve gives a Gaussian distribution of width $\sigma = 1$, normalised to have equal surface to the histogram. The RMSD is calculated using Eq. (3).

Title Page

Abstract | Introduction

Conclusions | References

Tables | Figures

|◄ | ►|

◄ | ►

Back | Close

Full Screen / Esc

Printer-friendly Version

Interactive Discussion
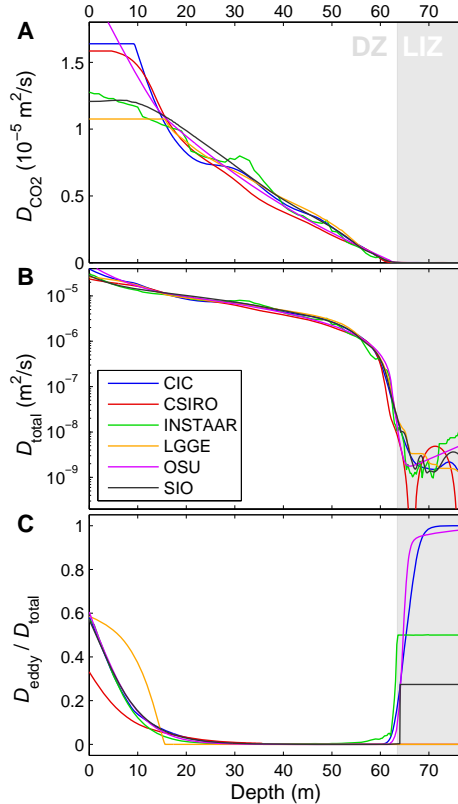
Fig. 5. (A) CO_2 molecular diffusivity profile with depth $D_{CO_2}(z)$ for the EU borehole. **(B)** Semi-log plot of the total CO_2 diffusivity profile $D_{total}(z) = D_{CO_2}(z) + D_{eddy}$. **(C)** Plot of $D_{eddy}(z)/D_{total}(z)$. Eddy diffusion near the surface corresponds to convective mixing; in the LIZ some of the models include dispersive mixing. The CSIRO model has zero eddy diffusivity in the LIZ; the line is not visible as the LGGE-GIPSA model is plotted on top of it.
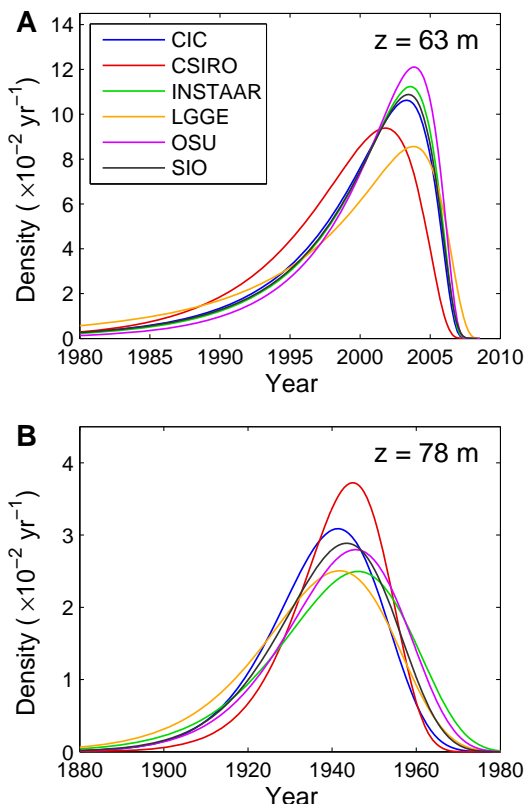
Fig. 6. EU borehole modeled CO_2 age distribution densities for **(A)** depth $z = 63\,\text{m}$ (lock-in depth) and **(B)** depth $z = 78\,\text{m}$ (bottom of LIZ). On the horizontal axis are calendar years C.E.; decimal sampling year is 2008.54 (i.e. mid July). Age distributions are calculated by applying a surface forcing which is unity for $0.2 \leq t < 0.4\,\text{yr}$, and zero elsewhere.
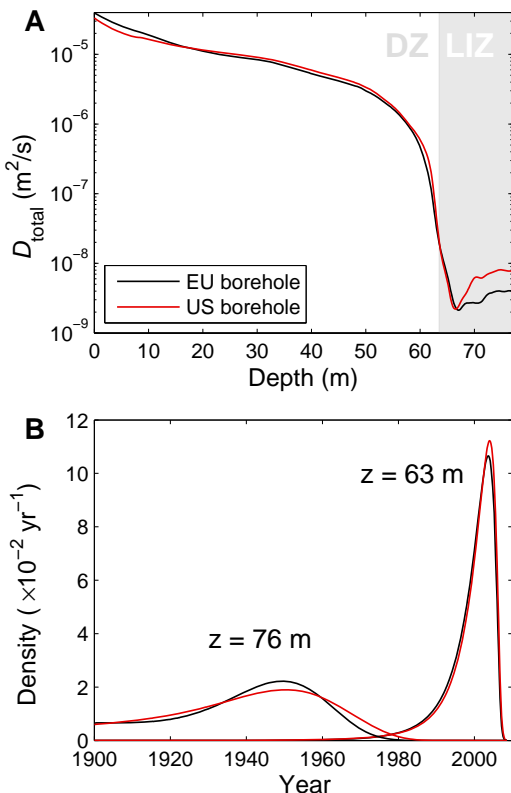
Fig. 7. Comparison between the EU and US boreholes. **(A)** Semi-log plot of the total CO_2 diffusivity profile $D_{total}(z) = D_{CO_2}(z) + D_{eddy}$ averaged over all six firn models. **(B)** Age distributions at depths $z = 63$ m (lock-in depth) and $z = 76$ m (bottom of LIZ) averaged over five firn models. The CSIRO model is excluded in the age distribution comparison as the US age distribution at $z = 76$ m is unreliable (Supplement).
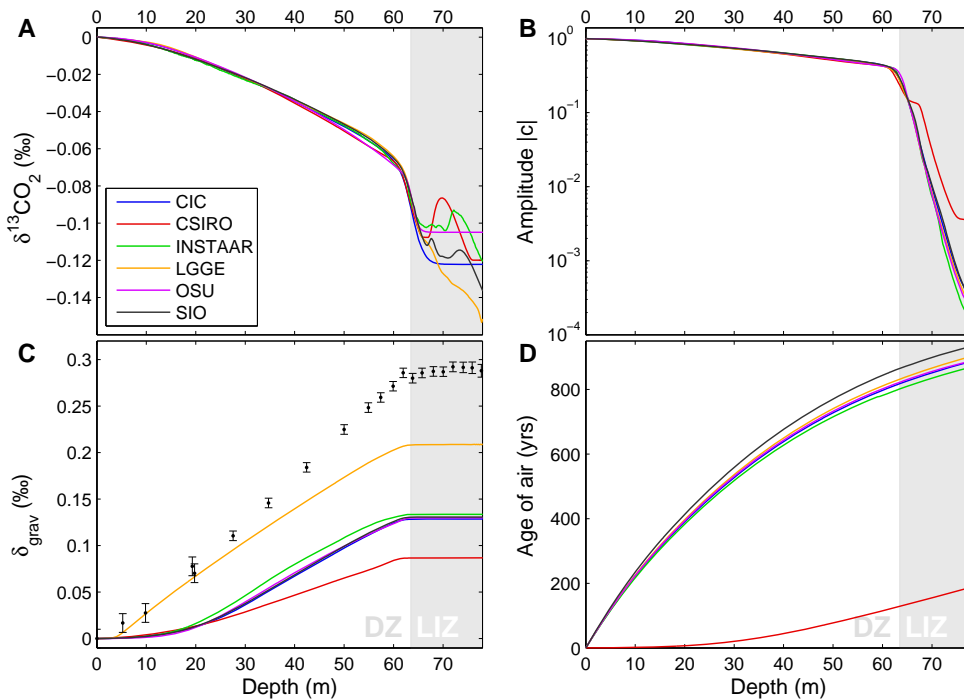
Fig. 8. Model comparison using the four diagnostic scenarios and diffusivity tuned to the EU borehole data. **(A)** Scenario I: diffusive fractionation for a hypothetical monotonic CO_2 increase. **(B)** Scenario II: attenuation of a 15 yr period sinusoidal CO_2 forcing with depth. **(C)** Scenario III: gravitational enrichment for gas X with $D_X^0 = 0.025 D_{CO_2}^0$. Data show gravitational enrichment of $^{15}N_2$ corrected for the effect of thermal diffusion. See Supplement for details. **(D)** Scenario IV: mean age of gas Y when using advective transport only ($D_Y^0 = 0$, i.e. diffusion is absent). With the exception of S-III all scenarios were run with the effect of gravity turned off.

Title Page

Abstract | Introduction

Conclusions | References

Tables | Figures

|◄ | ►|

◄ | ►

Back | Close

Full Screen / Esc

Printer-friendly Version

Interactive Discussion